

Signatures of exciton orbits in quantum mechanical recurrence spectra of Cu_2O

Jan Ertl,^{1,2} Michael Marquardt,¹ Moritz Schumacher,¹ Patric Rommel,¹ Jörg Main,^{1,*} and Manfred Bayer²

¹*Institut für Theoretische Physik I, Universität Stuttgart, 70550 Stuttgart, Germany*

²*Experimentelle Physik 2, Technische Universität Dortmund, 44221 Dortmund, Germany*

(Dated: July 25, 2022)

The seminal work by T. Kazimierczuk et al. [Nature **514**, 343 (2014)] has shown the existence of highly excited exciton states in a regime, where the correspondence principle is applicable and quantum mechanics turns into classical mechanics, however, any interpretation of exciton spectra based on a classical approach to excitons is still missing. Here, we close this gap by computing and comparing quantum mechanical and semiclassical recurrence spectra of cuprous oxide. We show that the quantum mechanical recurrence spectra exhibit peaks, which, by application of semiclassical theories and a scaling transformation, can be directly related to classical periodic exciton orbits. The application of semiclassical theories to exciton physics requires the detailed analysis of the classical exciton dynamics, including *three-dimensional* orbits, which strongly deviate from hydrogenlike Keplerian orbits. Our findings illuminate important aspects of excitons in semiconductors by directly relating the quantum mechanical band-structure splittings of excitons to the corresponding classical exciton dynamics.

Excitons are atom-like states in semiconductors formed by an electron and a positively charged hole. They are created by exciting an electron from the valence band into the conduction band, where the electron forms a bound hydrogenlike state with the hole remaining in the valence band [1, 2]. Since the experimental observation of giant Rydberg excitons with principal quantum numbers up to $n = 25$ in Cu_2O by Kazimierczuk et al. [3] the exciton physics of cuprous oxide has attracted a strongly increasing interest, both experimentally [3–6] and theoretically [4–8]. In particular, the impact of the valence band structure causes significant deviations of the exciton spectra from a simple hydrogenlike model, which have now been investigated in great detail [4–7].

For the hydrogen atom the connection of Rydberg spectra to classical Keplerian orbits is well established by the Bohr-Sommerfeld model. Semiclassical trace formulas [9, 10] provide the link between quantum spectra and classical dynamics of both regular and chaotic systems, and are the foundation for the understanding of level-spacing dynamics [11]. For example, the diamagnetic Kepler problem has served as a prototype system for the study of *quantum chaos*, i.e., the effects of a classical chaotic dynamics on quantum spectra [12, 13]. Due to the additional spin degrees of freedom in the semiconductor and the strong, non-negligible spin-orbit interaction the existence of an exciton dynamics for quasiparticles similar as for electrons in hydrogen atoms is not obvious. A first step on a semiclassical description of Rydberg excitons in Cu_2O has been made in Ref. [14] by proposing a classical model using an adiabatic approach that separates the fast spin dynamics and the slow electron-hole dynamics. By constructing action variables for the exciton dynamics in certain symmetry planes of the crystal allowed energy regions for the existence of exciton states could be obtained. This gives a first hint for the validity of a semiclassical approach, however, a direct verifica-

tion of a classical exciton dynamics is still missing. By computing the quantum mechanical recurrence spectra and comparing them with the classical and semiclassical results, we reveal, the existence and meaningfulness of a classical exciton dynamics. Direct signatures of exciton orbits obtained in quantum mechanical exciton recurrence spectra provide an intuitive picture for the understanding of excitons in Cu_2O .

The investigation of the phase space topology with similar methods as introduced by Gekle et al. [15, 16] for the hydrogen atom in crossed electric and magnetic fields, reveals a mostly regular or near-integrable exciton dynamics with periodic orbits on one- to three-dimensional tori. Here, we establish the connection between the fine-structure splitting of excitons in quantum spectra of the yellow series of Cu_2O and the corresponding classical exciton dynamics. According to semiclassical theories [9, 10], the frequencies of the oscillations are determined by the action of the periodic orbits, and the amplitudes are related to stability properties of the orbits at a given energy. Performing a Fourier transform of the density of states from energy to time domain results in a recurrence spectrum which exhibits peaks at periods that can be assigned to classical orbits [17]. For systems exhibiting an appropriate scaling property the peaks in the recurrence spectrum become sharp δ peaks [18]. To this aim we apply a scaling technique and calculate the classical dynamics of the system. The obtained periodic exciton orbits perfectly explain the observed structures in the quantum mechanical recurrence spectra, and thus provide a deeper physical understanding of excitons in semiconductors.

A full description of excitons in cuprous oxide needs to consider the cubic O_h symmetry of the system. Introducing relative and center-of-mass coordinates for the electron and hole and neglecting the center-of-mass momentum, the Hamiltonian for excitons in cuprous oxide

is given by [7, 19, 20]

$$H = E_g + H_{\text{kin}}(\mathbf{p}, \hat{\mathbf{I}}, \hat{\mathbf{S}}_h) - \frac{e^2}{4\pi\epsilon_0\epsilon|\mathbf{r}|} + H_{\text{SO}}, \quad (1)$$

with the relative coordinates \mathbf{r} and momenta \mathbf{p} and the vector operators $\hat{\mathbf{I}}, \hat{\mathbf{S}}_h$ for angular momenta $I = 1$ and $S_h = 1/2$. Here, the first term $E_g = 2.17208$ eV is the gap energy between the uppermost valence band and the lowest conduction band [3]. The second term

$$\begin{aligned} H_{\text{kin}}(\mathbf{p}, \hat{\mathbf{I}}, \hat{\mathbf{S}}_h) &= \frac{\gamma'_1}{2m_0}\mathbf{p}^2 + \frac{1}{2\hbar^2 m_0} [4\gamma_2\hbar^2\mathbf{p}^2 \\ &- 6\gamma_2(p_1^2\hat{I}_1^2 + \text{c.p.}) - 12\gamma_3(\{p_1, p_2\}\{\hat{I}_1, \hat{I}_2\} + \text{c.p.}) \\ &- 12\eta_2(p_1^2\hat{I}_1\hat{S}_{h1} + \text{c.p.}) + 2(\eta_1 + 2\eta_2)\mathbf{p}^2(\hat{\mathbf{I}} \cdot \hat{\mathbf{S}}_h) \\ &- 12\eta_3(\{p_1, p_2\}(\hat{I}_1\hat{S}_{h2} + \hat{I}_2\hat{S}_{h1}) + \text{c.p.})], \end{aligned} \quad (2)$$

accounts for the kinetic energy of the electron and hole. It includes the cubic band structure, described by the quasispin $\hat{\mathbf{I}}$ and the hole spin $\hat{\mathbf{S}}_h$ with their components \hat{I}_i, \hat{S}_{hi} as well as the components of the momentum p_i . Furthermore, m_0 is the free-electron mass, $\{a, b\} = \frac{1}{2}(ab + ba)$ denotes the symmetrized product, c.p. stands for cyclic permutation, γ_i and η_i are the Luttinger parameters [5], and $\gamma'_1 = \gamma_1 + m_0/m_e = 2.77$. The third term in Eq. (1) is the screened Coulomb potential with the dielectric constant $\epsilon = 7.5$. The fourth term in Eq. (1) is the spin-orbit term

$$H_{\text{SO}} = \frac{2}{3}\Delta \left(1 + \frac{1}{\hbar^2} \hat{\mathbf{I}} \cdot \hat{\mathbf{S}}_h \right), \quad (3)$$

where $\Delta = 0.131$ eV is the spin-orbit coupling [5]. In our computations we use the same material parameters as given in Ref. [21], but neglect central-cell corrections [8, 22, 23], which can be justified for high principal quantum numbers in the semiclassical limit [24]. For a given energy the classical dynamics of the yellow exciton series can be calculated by using the adiabatic approach introduced in [14, 24].

Without the spin-orbit term (3) the Hamiltonian (1) does not depend on the energy when multiplied by n_{eff}^2 and performing a scaling transformation $\mathbf{r} = n_{\text{eff}}^2\tilde{\mathbf{r}}, \mathbf{p} = n_{\text{eff}}^{-1}\tilde{\mathbf{p}}$, with the effective quantum number n_{eff} given by $n_{\text{eff}}^2 \equiv E_{\text{Ryd}}/(E_g - E)$ with $E_{\text{Ryd}} = 13.6\text{eV}/(\gamma'_1\epsilon^2) \approx 87\text{meV}$ the Rydberg energy of cuprous oxide, which means that the classical dynamics is the same for all values of n_{eff} . The non-scaled action S is connected to the scaled value \tilde{S} by a simple linear scaling $S_{\text{po}}(n_{\text{eff}}) = \tilde{S}_{\text{po}}n_{\text{eff}}$. In semiclassical theories the density of states for systems with such a scaling property can be expressed as a Fourier series in the scaled action \tilde{S}_{po} [17, 18],

$$\varrho(n_{\text{eff}}) = \varrho_0(n_{\text{eff}}) + \text{Re} \sum_{\text{po}} \mathcal{A}_{\text{po}} \exp\left(i\tilde{S}_{\text{po}}n_{\text{eff}}/\hbar\right), \quad (4)$$

with $\varrho_0(n_{\text{eff}})$ the average density of states. The sinusoidal fluctuations of the density are related to the periodic orbits (po) of the classical system with \mathcal{A}_{po} and \tilde{S}_{po} the amplitude (including the Maslov index) and the scaled action of the orbits, respectively.

To recover the scaling property for the Hamiltonian we introduce an energy-dependent coupling parameter $\tilde{\Delta}$, i.e.,

$$\Delta \rightarrow \tilde{\Delta} = \frac{n_0^2}{n_{\text{eff}}^2} \Delta, \quad (5)$$

with a fixed parameter n_0 . Note that the replacement (5) is not possible in an experiment, however, a tunable spin-orbit coupling Δ has already been used for the theoretical investigation of the exchange interaction in the yellow exciton series [23]. The classical dynamics is then that of $n_{\text{eff}} = n_0$. Using the adiabatic approach [14, 24] and choosing the lowest-lying energy surface in momentum space corresponding to the yellow exciton series classical exciton orbits can be obtained by numerical integration of Hamilton's equations of motion for the relative coordinates and momenta. In most parts of the phase space we observe a regular dynamics of the excitons on one- to three-dimensional tori. Periodic orbits on these tori can be described by one to three integer winding numbers M_i . The number of winding numbers for the three-dimensional orbits can be reduced to an effective two-dimensional description by two winding numbers M_1 and M_2 [24]. The corresponding action variables are J_1 and J_2 . At given energy E they are related by the function $g_E(J_1) = J_2$, which can be used to compute the semiclassical amplitudes of periodic orbits on resonant tori [9, 25]. In addition the stability eigenvalues λ_{po} , which describe the linearized response of a periodic orbit to a small perturbation are required for the calculation of the semiclassical amplitudes in Eq. (4). Since only one pair of stability eigenvalues shows deviations from the integrable behavior for the majority of orbits we use a mixed approach combining the amplitudes of the Berry-Tabor formula for a two-dimensional system [9, 25] with the contribution of the stability eigenvalues λ_{po} and $1/\lambda_{\text{po}}$ for the unstable direction from Gutzwiller's trace formula [10], resulting in the equation

$$|\mathcal{A}_{\text{po}}| = \frac{1}{\pi\hbar} \frac{1}{\sqrt{|\lambda_{\text{po}} + 1/\lambda_{\text{po}} - 2|}} \frac{\tilde{S}_{\text{po}}}{\sqrt{\hbar M_2^3 |g''_E|}} \quad (6)$$

for the periodic-orbit amplitudes [24]. For the computation of the amplitudes of the isolated nearly circular orbits we resort directly to Gutzwiller's trace formula.

In the quantum mechanical case the operators for position and momentum read $\hat{\mathbf{r}} = \tilde{\mathbf{r}}, \hat{\mathbf{p}} = -i\hbar_{\text{eff}}\nabla_{\tilde{\mathbf{r}}}$, with $\hbar_{\text{eff}} = \hbar/n_{\text{eff}}$ an effective Planck constant [26]. The Schrödinger equation for cuprous oxide is now trans-

formed to the generalized eigenvalue problem

$$\left[\frac{e^2}{4\pi\epsilon_0\epsilon|\tilde{\mathbf{r}}|} - n_0^2 H_{\text{SO}} - E_{\text{Ryd}} \right] |\Psi\rangle = \hbar_{\text{eff}}^2 H_{\text{kin}} |\Psi\rangle \quad (7)$$

for the squared effective Planck constant, i.e. $\lambda = \hbar_{\text{eff}}^2$, and thus the effective quantum number n_{eff} . Eq. (7) is solved numerically by using a complete set of basis states $|NLJFM_F\rangle$ with Coulomb-Sturmian radial functions $U_{NL}(r)$ [26].

The decisive point of the scaling is that the eigenvalues in Eq. (7) correspond to the effective Planck constant $\hbar_{\text{eff}} = \hbar/n_{\text{eff}}$, i.e., the eigenstates approach the semiclassical limit with increasing eigenvalues n_{eff} , but the classical exciton dynamics corresponding to the spectrum does not depend on this effective Planck constant, and thus stays the same for all states of the scaled spectrum. The classical exciton dynamics is that of the non-scaled Hamiltonian (1) ($n_{\text{eff}} = n_0$ in Eq. (5)) at energy $E = E_g - E_{\text{Ryd}}/n_0^2$, and is thus controlled via the parameter n_0 in Eqs. (5) and (7). The fluctuations of the scaled quantum spectra obtained from Eq. (7) can be analyzed by Fourier transform in the variable n_{eff} and, via the semiclassical result (4), should provide δ peaks at frequencies given by the scaled actions \tilde{S}_{po} of the periodic orbits of the corresponding classical exciton dynamics.

In the following all parameters are given in exciton-Hartree units which are obtained by setting $\hbar = e = m_0/\gamma'_1 = 1/(4\pi\epsilon_0\epsilon) = 1$. For the presentation of the results we focus on $n_0 = 5$, i.e., a principal quantum number, which is high enough that the adiabatic approach is valid, but low enough that the secular motion of the classical exciton orbits, which decreases with increasing n_0 , is sufficiently fast [24]. Numerical diagonalization of the generalized eigenvalue problem (7) provides the scaled quantum mechanical spectrum for n_{eff} displayed in Fig. 1(a) showing nicely the fine structure splittings. Due to the scaling property introduced in Eq. (5) the spectrum differs from the physical (non-scaled) spectrum. The ratio of the scaled spin-orbit splitting $\tilde{\Delta}$ to the physical value Δ is shown in the upper axis of Fig. 1(a). In the vicinity of $n_{\text{eff}} \rightarrow n_0$ the scaled spin-orbit splitting and the physical value coincide leading to a good agreement of physical and scaled spectra in this energy range. Contrary to the physical spectrum, the scaled spectrum can be understood directly in terms of classical orbits, because the semiclassical density of states for the scaled systems is given as a Fourier series with the semiclassical amplitudes \mathcal{A}_{po} at positions \tilde{S}_{po} .

The scaled quantum spectrum shown in Fig. 1(a) is a sum of δ distributions, and thus the Fourier transform (FT) can easily be carried out analytically. The resulting Fourier spectrum is presented as black solid line in Fig. 1(b). It exhibits a large number of sharp peaks with increasing density as a function of \tilde{S} . The peaks should approach δ functions, i.e., become infinitely narrow for

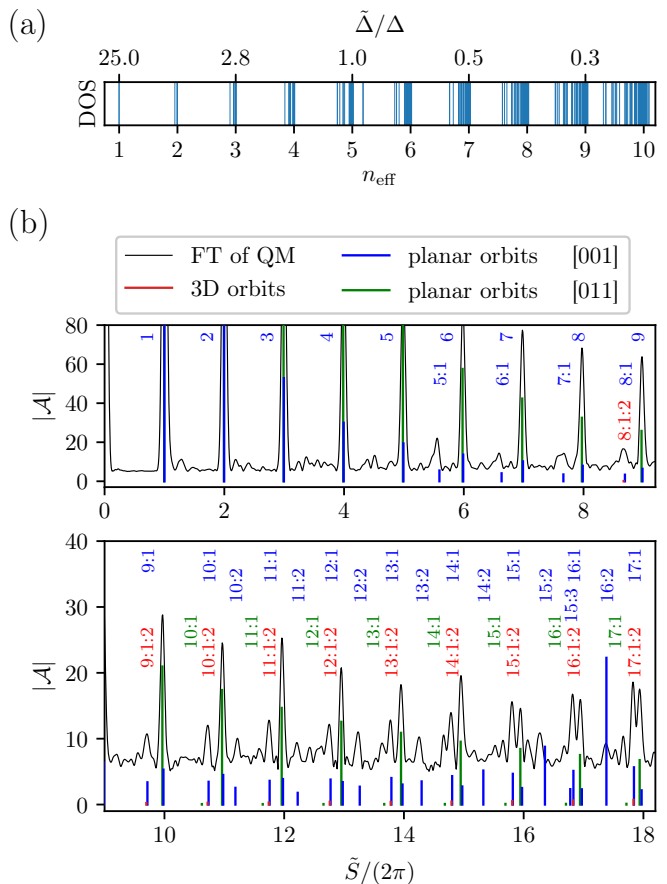


FIG. 1. (a) Part of the scaled quantum mechanical density of states for $n_0 = 5$. (b) Quantum mechanical exciton recurrence spectrum (black solid line, with zero line shifted for better visibility) obtained by Fourier transform (FT) of the density of states shown in (a) and the semiclassical recurrence spectrum (colored bars). The peaks corresponding to one or multiple repetitions of nearly circular orbits are labeled with a single winding number M_1 . Two winding numbers $M_1:M_2$ indicate planar orbits in one of the two different symmetry planes of the crystal, and fully three-dimensional orbits are marked by three winding numbers $M_1:M_2:M_3$. The observed structures agree very well with the semiclassical results.

the Fourier transform of an infinitely long scaled quantum spectrum with $n_{\text{eff}} \rightarrow \infty$. However, for finite length, resulting from the diagonalization of the truncated generalized eigenvalue problem (7), the peaks are broadened and side peaks may occur. To suppress these features we use a Gaussian window function as an envelope when performing the Fourier transform [26].

For comparison, the semiclassical results are shown in Fig. 1(b) as colored peaks at the positions $\tilde{S}_{\text{po}}/2\pi$ of the periodic orbits. The peak heights mark the absolute values $|\mathcal{A}_{\text{po}}|$ of the semiclassical amplitudes. The peaks are labeled by the one to three winding numbers M_i of the corresponding periodic orbits moving on one- to three-dimensional tori. As can be seen in Fig. 1(b), the quantum mechanical and semiclassical exciton recur-

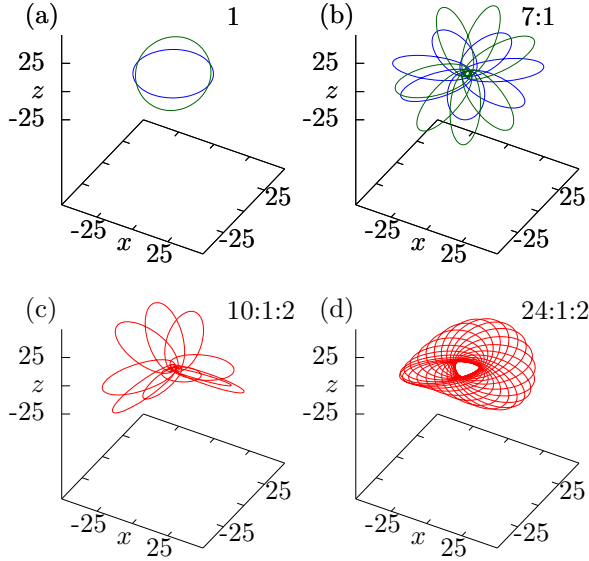


FIG. 2. (a) Nearly circular orbits with winding number $M_1 = 1$ and (b) planar orbits with winding numbers $M_1:M_2 = 7:1$ in the two different symmetry planes of the crystal. (c) and (d): Two examples of fully three-dimensional orbits with winding numbers $M_1:M_2:M_3$. The colors are the same as in Fig. 1.

rence spectra agree very well. At low action ($\tilde{S}/2\pi \lesssim 5$) the peaks solely belong to one or multiple recurrences of the two shortest periodic exciton orbits, viz. the nearly circular orbits in the planes perpendicular to the [001] and [011] axes, moving on one-dimensional tori labeled by a single winding number $M_1 = 1, 2, 3, \dots$. These orbits are shown in Fig. 2(a). At higher action ($\tilde{S}/2\pi \gtrsim 5$) the recurrence spectrum becomes more and more complicated due to the appearance of additional peaks belonging to exciton orbits on two-dimensional tori located in the planes perpendicular to the [001] and [011] axes (marked by two winding numbers $M_1:M_2$) or fully three-dimensional orbits with winding numbers $M_1:M_2:M_3$. The 2D orbits with $M_1:M_2 = 7:1$ in the symmetry planes of the crystal are shown in Fig. 2(b). Two fully 3D exciton orbits are illustrated in Fig. 2(c) and (d).

The structure of the classical exciton dynamics is illustrated in more detail in Fig. 3, where the classical action \tilde{S}_{po} of the period orbits is shown as function of the ratio of the winding numbers M_1/M_2 . For better visibility, the actions are normalized by the actions $\tilde{S}_{\perp[011]}$ of the corresponding orbits with the same winding numbers M_1 and M_2 in the plane perpendicular to the [011] axis. Therefore, by construction, the periodic orbits in the plane perpendicular to the [011] axis are located on the straight line at $\tilde{S}_{\text{po}}/\tilde{S}_{\perp[011]} = 1$. These orbits lie on a 2D torus in phase space. With increasing ratio M_1/M_2 they converge at $M_1/M_2 \approx 68.8$ to the nearly circular

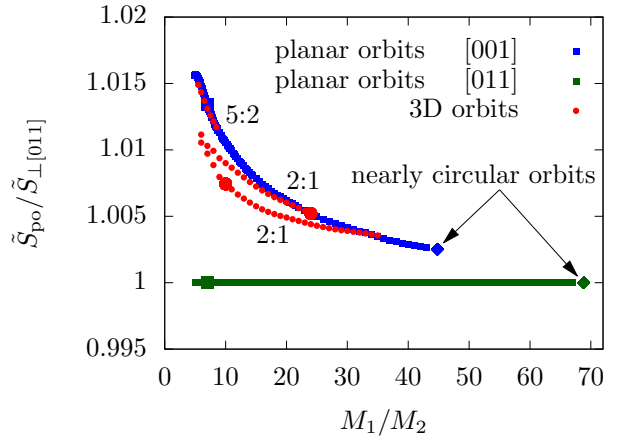


FIG. 3. Actions \tilde{S}_{po} of periodic orbits as function of the ratio of winding numbers M_1/M_2 . The actions are normalized by the actions $\tilde{S}_{\perp[011]}$ of the corresponding orbits with the same winding numbers M_1 and M_2 in the plane perpendicular to the [011] axis. The two-dimensional orbits approach the action of the nearly circular orbit (indicated by rhombi) of the corresponding plane with increasing M_1/M_2 . Some three-dimensional orbits with marked ratio $M_3:M_2$ are located in the area enclosed by orbits in the two different symmetry planes of the O_h group. The orbits shown in Fig. 2 are highlighted by larger symbols.

orbit in the symmetry plane perpendicular to [011]. This point in Fig. 3 thus represents a limiting 1D torus in phase space indicated by the green rhombus. In a similar way the periodic orbits perpendicular to the [001] axis, lying on a different 2D torus in phase space, are located on the upper line in Fig. 3 with the limiting nearly circular orbit on a 1D torus at $M_1/M_2 \approx 44.8$ shown as blue rhombus. In between the orbits on the two limiting 2D tori the periodic orbits on the 3D tori are located. Subsets of these orbits with winding number $M_2 = 1$ or 2 and ratios $M_3:M_2 = 2:1$ or $5:2$ are marked by red dots in Fig. 3. The three-dimensional orbits fill the area between the limiting 2D tori more densely when longer periodic orbits with more complicated ratios of the winding numbers are considered. As can be seen in Fig. 3, the classical action of periodic orbits with the same winding numbers M_1 and M_2 differ by less than 2%. This causes a clustering of several orbits in the recurrence spectra in Fig. 1(b). In these clusters the peaks at the highest action belong to the two-dimensional orbits in the (mostly) stable symmetry plane perpendicular to the [001] axis and its equivalents. Typically, these peaks exhibit the highest semiclassical amplitude within the cluster. At slightly lower action one finds unstable three-dimensional orbits, and the peak with lowest action of the cluster belongs to a two-dimensional orbit in the plane perpendicular to the [011] axis.

In summary, we have found signatures of exciton orbits in quantum mechanical recurrence spectra of cuprous

oxide. We have revealed the classical phase space structure of yellow excitons in cuprous oxide and observed recurrence peaks in Fourier transform quantum spectra, which, by application of semiclassical theories can be directly related to two-dimensional periodic orbits in symmetry planes of the crystal or fully three-dimensional periodic orbits. The results have been obtained by using an adiabatic approach for the classical exciton dynamics and by application of a scaling technique to the quantum spectra. Considering these approximations and that the Bohr-Sommerfeld model already fails to predict the energy levels of the helium atom, it is remarkable that a classical picture is capable of describing the spectral features of excitons in Cu_2O . Here, we have focused on the dynamics of Rydberg excitons with principal quantum number $n = 5$ in the (non-scaled) Cu_2O crystal. The analysis will be extended to other dynamics regimes by varying n_0 . It will also be interesting to investigate the classical and semiclassical dynamics of magnetoexcitons [27, 28] in cuprous oxide. Furthermore, the classical model intrinsically exhibits a dipole moment which could provide a starting point to describe and better understand interactions between Rydberg excitons such as scattering processes between Rydberg excitons [29, 30], the Rydberg blockade [31], and the possible existence of an exciton molecule [32] in analogy to Rydberg molecules [33, 34].

This work was supported by Deutsche Forschungsgemeinschaft (DFG) through Grant No. MA1639/16-1 and through the International Collaborative Research Centre (ICRC) TRR 160 (project A8).

* Email: main@itp1.uni-stuttgart.de

- [1] E. F. Gross, Optical spectrum of excitons in the crystal lattice, *Il Nuovo Cimento* (1955-1965) **3**, 672 (1956).
- [2] J. M. Luttinger, Quantum theory of cyclotron resonance in semiconductors: General theory, *Phys. Rev.* **102**, 1030 (1956).
- [3] T. Kazimierczuk, D. Fröhlich, S. Scheel, H. Stolz, and M. Bayer, Giant Rydberg excitons in the copper oxide Cu_2O , *Nature* **514**, 343 (2014).
- [4] F. Schöne, S.-O. Krüger, P. Grünwald, M. Aßmann, J. Heckötter, J. Thewes, H. Stolz, D. Fröhlich, M. Bayer, and S. Scheel, Coupled valence band dispersions and the quantum defect of excitons in Cu_2O , *Journal of Physics B: Atomic, Molecular and Optical Physics* **49**, 134003 (2016).
- [5] F. Schöne, S.-O. Krüger, P. Grünwald, H. Stolz, S. Scheel, M. Aßmann, J. Heckötter, J. Thewes, D. Fröhlich, and M. Bayer, Deviations of the exciton level spectrum in Cu_2O from the hydrogen series, *Phys. Rev. B* **93**, 075203 (2016).
- [6] J. Thewes, J. Heckötter, T. Kazimierczuk, M. Aßmann, D. Fröhlich, M. Bayer, M. A. Semina, and M. M. Glazov, Observation of high angular momentum excitons in cuprous oxide, *Phys. Rev. Lett.* **115**, 027402 (2015).
- [7] F. Schweiner, J. Main, M. Feldmaier, G. Wunner, and C. Uihlein, Impact of the valence band structure of Cu_2O on excitonic spectra, *Phys. Rev. B* **93**, 195203 (2016).
- [8] F. Schweiner, J. Main, G. Wunner, and C. Uihlein, Even exciton series in Cu_2O , *Phys. Rev. B* **95**, 195201 (2017).
- [9] M. V. Berry and M. Tabor, Closed orbits and the regular bound spectrum, *Proc. R. Soc. Lond. A* **349**, 101 (1976).
- [10] M. C. Gutzwiller, *Chaos in Classical and Quantum Mechanics* (Springer, New York, 1990).
- [11] F. Haake, S. Gnutzmann, and M. Kuś, *Quantum Signatures of Chaos, Fourth Edition*, Springer Series in Synergetics (Springer, Cham, 2018).
- [12] H. Friedrich and H. Wintgen, The hydrogen atom in a uniform magnetic field – An example of chaos, *Physics Reports* **183**, 37–79 (1989).
- [13] H. Hasegawa, M. Robnik, and G. Wunner, Classical and Quantal Chaos in the Diamagnetic Kepler Problem, *Progress of Theoretical Physics Supplement* **98**, 198 (1989).
- [14] J. Ertl, P. Rommel, M. Mom, J. Main, and M. Bayer, Classical and semiclassical description of Rydberg excitons in cuprous oxide, *Phys. Rev. B* **101**, 241201(R) (2020).
- [15] S. Gekle, J. Main, T. Bartsch, and T. Uzer, Extracting multidimensional phase space topology from periodic orbits, *Phys. Rev. Lett.* **97**, 104101 (2006).
- [16] S. Gekle, J. Main, T. Bartsch, and T. Uzer, Hydrogen atom in crossed electric and magnetic fields: Phase space topology and torus quantization via periodic orbits, *Phys. Rev. A* **75**, 023406 (2007).
- [17] See Sec. I of Supplemental Material at [URL to be inserted] for more details on semiclassical periodic orbit theory including semiclassical density of states, scaling techniques, and recurrence spectra, which includes the additional Refs. [35, 36].
- [18] J. Main, Use of harmonic inversion techniques in semiclassical quantization and analysis of quantum spectra, *Phys. Rep.* **316**, 233–338 (1999).
- [19] N. O. Lipari and M. Altarelli, Theory of indirect excitons in semiconductors, *Phys. Rev. B* **15**, 4883 (1977).
- [20] C. Uihlein, D. Fröhlich, and R. Kenklies, Investigation of exciton fine structure in Cu_2O , *Phys. Rev. B* **23**, 2731 (1981).
- [21] P. Rommel, P. Zielinski, and J. Main, Green exciton series in cuprous oxide, *Phys. Rev. B* **101**, 075208 (2020).
- [22] A. Farenbruch, D. Fröhlich, D. R. Yakovlev, and M. Bayer, Rydberg series of dark excitons in Cu_2O , *Phys. Rev. Lett.* **125**, 207402 (2020).
- [23] P. Rommel, J. Main, A. Farenbruch, D. R. Yakovlev, and M. Bayer, Exchange interaction in the yellow exciton series of cuprous oxide, *Phys. Rev. B* **103**, 075202 (2021).
- [24] See Sec. II of Supplemental Material at [URL to be inserted] for more details on the computation of classical dynamics and the application of semiclassical methods for excitons in cuprous oxide, which includes the additional Ref. [37].
- [25] S. Tomsovic, M. Grinberg, and D. Ullmo, Semiclassical trace formulas of near-integrable systems: Resonances, *Phys. Rev. Lett.* **75**, 4346 (1995).
- [26] See Sec. III of Supplemental Material at [URL to be inserted] for more details on the computation of the scaled quantum mechanical density of states and scaled recurrence spectra for excitons in cuprous oxide, which includes the additional Refs. [38–42].

- [27] F. Schweiner, J. Main, G. Wunner, M. Freitag, J. Heckötter, C. Uihlein, M. Aßmann, D. Fröhlich, and M. Bayer, Magnetoexcitons in cuprous oxide, *Phys. Rev. B* **95**, 035202 (2017).
- [28] F. Schweiner, J. Main, and G. Wunner, Magnetoexcitons break antiunitary symmetries, *Phys. Rev. Lett.* **118**, 046401 (2017).
- [29] Y. Hefetz, X.-C. Zhang, and A. V. Nurmikko, Observation of exciton-exciton scattering in Cu_2O by time-resolved photomodulation spectroscopy, *Phys. Rev. B* **31**, 5371 (1985).
- [30] J. Shumway and D. M. Ceperley, Quantum Monte Carlo treatment of elastic exciton-exciton scattering, *Phys. Rev. B* **63**, 165209 (2001).
- [31] J. Heckötter, V. Walther, S. Scheel, M. Bayer, T. Pohl, and M. Aßmann, Asymmetric Rydberg blockade of giant excitons in Cuprous Oxide, *Nat. Commun.* **12**, 3556 (2021).
- [32] F. Bassani and M. Rovere, Biexciton binding energy in Cu_2O , *Solid State Commun.* **19**, 887 (1976).
- [33] V. Bendkowsky, B. Butscher, J. Nipper, J. P. Shaffer, R. Löw, and T. Pfau, Observation of ultralong-range Rydberg molecules, *Nature* **458**, 1005 (2009).
- [34] A. Junginger, J. Main, and G. Wunner, Quantum-classical model for the formation of Rydberg molecules, *Phys. Rev. A* **86**, 012713 (2012).
- [35] P. Cvitanović and B. Eckhardt, Periodic-orbit quantization of chaotic systems, *Phys. Rev. Lett.* **63**, 823 (1989).
- [36] A. Holle, J. Main, G. Wiebusch, H. Rottke, and K. H. Welge, Quasi-Landau spectrum of the chaotic diamagnetic hydrogen atom, *Phys. Rev. Lett.* **61**, 161 (1988).
- [37] M. Schumacher, *Semiclassical analysis and interpretation of quantum mechanically computed Cu_2O exciton spectra*, Master's thesis, Universität Stuttgart (2021).
- [38] M. A. Caprio, P. Maris, and J. P. Vary, Coulomb-Sturmian basis for the nuclear many-body problem, *Phys. Rev. C* **86**, 034312 (2012).
- [39] B. Klahn and W. A. Bingel, The convergence of the Rayleigh-Ritz method in quantum chemistry I., *Theoretica Chimica Acta* **44**, 9 (1977).
- [40] B. Klahn and W. A. Bingel, The convergence of the Rayleigh-Ritz method in quantum chemistry II., *Theoretica Chimica Acta* **44**, 27 (1977).
- [41] G. Koster, J. Dimmock, R. Wheeler, and H. Statz, *Properties of the thirty-two point groups*, Massachusetts Institute of Technology Press research monograph (M.I.T. Press, Cambridge, 1963).
- [42] E. Anderson, Z. Bai, C. Bischof, S. Blackford, J. Demmel, J. Dongarra, J. D. Croz, A. Greenbaum, S. Hammarling, and A. McKenney, *LAPACK Users' Guide, Third edition* (Society for Industrial and Applied Mathematics, Philadelphia, 1999).

Supplemental material for “Signatures of exciton orbits in quantum mechanical recurrence spectra of Cu₂O”

Jan Ertl,^{1,2} Michael Marquardt,¹ Moritz Schumacher,¹ Patric Rommel,¹ Jörg Main,^{1,*} and Manfred Bayer²

¹*Institut für Theoretische Physik I, Universität Stuttgart, 70550 Stuttgart, Germany*

²*Experimentelle Physik 2, Technische Universität Dortmund, 44221 Dortmund, Germany*

In this Supplemental Material, we provide a detailed description of the methods used in the primary text.

I. PERIODIC ORBIT THEORY

A. Semiclassical density of states

In semiclassical theories [1–3] the density of states is given by

$$\varrho_{\text{sc}}(E) = \varrho_0(E) + \sum_{\text{po}} \mathcal{A}_{\text{po}} \cos\left(S_{\text{po}}(E)/\hbar - \frac{\pi}{2}\mu_{\text{po}}\right), \quad (1)$$

with $\varrho_0(E)$ the average density of states. The sinusoidal fluctuations of the density of states are related to the periodic orbits of the classical system with \mathcal{A}_{po} , S_{po} , and μ_{po} the amplitude, action, and Maslov index of the orbits, respectively. In this treatment integrable and non-integrable systems must be distinguished.

The dynamics of integrable systems is regular and the motion is confined to tori characterized by action-angle variables J_i and ϑ_i . The action variables

$$J_i = \frac{1}{2\pi} \oint_{\mathcal{C}_i} \mathbf{p} d\mathbf{r} \quad (2)$$

provide a set of constants of motion, where the integrals are evaluated along the independent paths \mathcal{C}_i on the torus obtained when the angle variable ϑ_i is varied from 0 to 2π while all other angle variables ϑ_j with $j \neq i$ are kept constant. The frequencies ω_i on the torus are given by

$$\omega_i = \frac{\partial H}{\partial J_i}. \quad (3)$$

When all frequency ratios are given by rational numbers the trajectories are periodic on resonant tori, otherwise they are quasi-periodic. The periodic orbits can be characterized by integer winding numbers M_i that are defined by the number of cycles along the paths \mathcal{C}_i needed until the periodic orbit returns to its initial position.

For two-dimensional integrable systems the density of states is given by the Berry-Tabor formula [1, 2]

$$\varrho_{\text{sc}}(E) = \varrho_0(E) + \frac{1}{\pi\hbar} \sum_M \frac{dS_M/dE}{\sqrt{\hbar M_2^3 |g'_E|}} \cos\left(S_M/\hbar - \frac{\pi}{2}\mu_M - \frac{\pi}{4}\right). \quad (4)$$

where $\mathbf{M} = (M_1, M_2)$ are the winding numbers of the periodic orbits with classical action $S_{\mathbf{M}}$ and Maslov index $\mu_{\mathbf{M}}$. The amplitudes of the oscillating terms in Eq. (4) involve the periods $dS_{\mathbf{M}}/dE$ of the periodic orbits, the winding number M_2 , and the second derivative of the function g_E , which connects the two action variables via $J_2 = g_E(J_1)$.

In non-integrable systems the periodic orbits are isolated. The semiclassical density of states is then given by Gutzwiller’s trace formula [3]

$$\varrho_{\text{sc}}(E) = \varrho_0(E) + \frac{1}{\pi\hbar} \sum_{\text{ppo}} \frac{dS_{\text{ppo}}/dE}{\sqrt{|\det(\mathbf{M}_{\text{ppo}} - \mathbf{1})|}} \cos\left(S_{\text{ppo}}/\hbar - \frac{\pi}{2}\mu_{\text{ppo}}\right), \quad (5)$$

where S_{ppo} is the action of the primitive periodic orbit, \mathbf{M}_{ppo} is the monodromy matrix that describes the stability properties of the periodic orbit in the directions orthogonal to the orbit, and μ_{ppo} is the Maslov index.

B. Scaling technique

For certain systems it is possible to introduce a scaling of the coordinates and momenta such that the phase space structure of the classical dynamics no longer depends on the energy E or an appropriately chosen scaling parameter. Examples are billiard systems [4] or the hydrogen atom in a magnetic field [5–7]. In such systems a scaling parameter

$$w = \frac{1}{\hbar_{\text{eff}}} = \frac{n_{\text{eff}}}{\hbar} \quad (6)$$

can be introduced such that the shape of the classical orbits does not depend on w and the classical action of periodic orbits depend linearly on w , i.e.,

$$S_{\text{po}}(w)/\hbar = \tilde{S}_{\text{po}} w, \quad (7)$$

with \tilde{S}_{po} the scaled action of the periodic orbit. The scaling parameter w plays the role of an inverse effective Planck constant \hbar_{eff} or an effective quantum number n_{eff} .

Changing the external parameter from energy to w and inserting Eq. (7) into the general form of the semiclassical trace formula (1) the semiclassical density of states can be written as a Fourier series

$$\varrho_{\text{sc}}(w) = \varrho_0(w) + \text{Re} \sum_{\text{po}} \mathcal{A}_{\text{po}} \exp\left(i\tilde{S}_{\text{po}} w\right), \quad (8)$$

* Email: main@itp1.uni-stuttgart.de

with constant periodic orbit parameters, where we have included the phase given by the Maslov index in the complex amplitude \mathcal{A}_{po} .

C. Scaled recurrence spectra

In the semiclassical density of states (8) of a scaled system the complete set of periodic orbits lead to a superposition of sinusoidal fluctuations. The contribution of individual orbits to the spectrum is therefore not visible directly, but can be extracted by a Fourier transform of the spectrum from energy to time domain, or in the scaled picture from the w to the scaled action domain. The scaled semiclassical recurrence spectrum

$$C_{\text{sc}}(\tilde{S}) = \sum_{\text{po}} \mathcal{A}_{\text{po}} \delta(\tilde{S} - \tilde{S}_{\text{po}}), \quad (9)$$

then exhibits peaks at the positions of the scaled actions \tilde{S}_{po} with amplitudes \mathcal{A}_{po} .

The semiclassical recurrence spectrum (9) can be directly compared with its quantum mechanical counterpart. For scaled systems the Schrödinger equation describes eigenstates at discrete values $w = w_k$ of the scaling parameter. The Fourier transform of the quantum mechanical density of states

$$\varrho_{\text{qm}}(w) = \sum_k \delta(w - w_k) \quad (10)$$

can be calculated analytically and yields the quantum mechanical recurrence spectrum

$$\begin{aligned} C_{\text{qm}}(\tilde{S}) &= \frac{1}{2\pi} \int \varrho_{\text{qm}}(w) e^{-i\tilde{S}w} dw \\ &= \frac{1}{2\pi} \sum_k e^{-i\tilde{S}w_k}. \end{aligned} \quad (11)$$

By comparing the quantum mechanical result (11) with Eq. (9) it becomes clear that also the quantum mechanical recurrence spectrum should provide recurrence peaks at positions \tilde{S} given by the scaled actions of the periodic orbits of the corresponding classical system. This allows for the interpretation of the quantum spectra in terms of classical orbits. More details on the application of the semiclassical approach and the scaling technique to excitons in cuprous oxide are given below.

II. CLASSICAL AND SEMICLASSICAL DESCRIPTION OF EXCITONS IN CUPROUS OXIDE

A. Scaling of the classical dynamics

Excitons in semiconductors like Cu_2O are atom-like states formed by an electron in the conduction band and

a positively charged hole in the valence band. Neglecting all details of the band structure an exciton can be described in a simple hydrogenlike model by the Hamiltonian

$$H = E_g + \frac{\gamma'_1}{2m_0} \mathbf{p}^2 - \frac{e^2}{4\pi\epsilon_0\epsilon|\mathbf{r}|}. \quad (12)$$

The first term $E_g = 2.17208 \text{ eV}$ is the gap energy between the uppermost valence band and the lowest conduction band [8] and \mathbf{r} and \mathbf{p} are the relative coordinates and corresponding momenta. Here, an appropriate scaling to make the dynamics energy-independent is given by

$$\mathbf{r} = n_{\text{eff}}^2 \tilde{\mathbf{r}}, \quad \mathbf{p} = \frac{1}{n_{\text{eff}}} \tilde{\mathbf{p}}, \quad (13)$$

where we introduced n_{eff} via $n_{\text{eff}}^2 \equiv E_{\text{Ryd}}/(E_g - E)$ with $E_{\text{Ryd}} = 13.6 \text{ eV}/(\gamma'_1 \epsilon^2) \approx 87 \text{ meV}$ the Rydberg energy of cuprous oxide. After subtracting E_g and multiplying with n_{eff}^2 the scaled Hamiltonian reads

$$\tilde{H} = n_{\text{eff}}^2 (H - E_g) = \frac{\gamma'_1}{2m_0} \tilde{\mathbf{p}}^2 - \frac{e^2}{4\pi\epsilon_0\epsilon|\tilde{\mathbf{r}}|} = -E_{\text{Ryd}} \quad (14)$$

and therefore the classical dynamics becomes independent of n_{eff} . The connection between non-scaled action S and scaled action \tilde{S} is then given by

$$S_{\text{po}}(n_{\text{eff}}) = \tilde{S}_{\text{po}} n_{\text{eff}}. \quad (15)$$

The semiclassical density of states therefore takes the form (8) when setting $w = n_{\text{eff}}/\hbar$, and the recurrence spectrum exhibits δ peaks at scaled actions \tilde{S}_{po} of multiple repetitions of Keplerian orbits corresponding to the hydrogenlike Coulomb problem.

The true exciton dynamics is much more complicated. A full description of excitons in cuprous oxide needs to include the cubic band structure of the crystal. This requires the replacement of the kinetic term in Eq. (12) by

$$\frac{\gamma'_1}{2m_0} \mathbf{p}^2 \rightarrow H_{\text{kin}}(\mathbf{p}, \hat{\mathbf{I}}, \hat{\mathbf{S}}_h) + H_{\text{SO}}(\hat{\mathbf{I}}, \hat{\mathbf{S}}_h), \quad (16)$$

with the vector operators $\hat{\mathbf{I}}$, $\hat{\mathbf{S}}_h$ for angular momenta $I = 1$ and $S_h = 1/2$. The kinetic terms can be split into the hydrogenlike term plus corrections due to the band structure $H_{\text{band}}(\mathbf{p}, \hat{\mathbf{I}}, \hat{\mathbf{S}}_h)$, i.e.

$$\begin{aligned} H_{\text{kin}}(\mathbf{p}, \hat{\mathbf{I}}, \hat{\mathbf{S}}_h) + H_{\text{SO}}(\hat{\mathbf{I}}, \hat{\mathbf{S}}_h) &= \frac{\gamma'_1}{2m_0} \mathbf{p}^2 + H_{\text{band}}(\mathbf{p}, \hat{\mathbf{I}}, \hat{\mathbf{S}}_h) \\ &= \frac{\gamma'_1}{2m_0} \mathbf{p}^2 + \frac{1}{2\hbar^2 m_0} [4\gamma_2 \hbar^2 \mathbf{p}^2 - 6\gamma_2 (p_1^2 \hat{I}_1 + \text{c.p.}) \\ &\quad - 12\gamma_3 (\{p_1, p_2\} \{\hat{I}_1, \hat{I}_2\} + \text{c.p.}) - 12\eta_2 (p_1^2 \hat{I}_1 \hat{S}_{h1} + \text{c.p.}) \\ &\quad + 2(\eta_1 + 2\eta_2) \mathbf{p}^2 (\hat{\mathbf{I}} \cdot \hat{\mathbf{S}}_h) - 12\eta_3 (\{p_1, p_2\} (\hat{I}_1 \hat{S}_{h2} \\ &\quad + \hat{I}_2 \hat{S}_{h1}) + \text{c.p.})] + H_{\text{SO}}(\hat{\mathbf{I}}, \hat{\mathbf{S}}_h). \end{aligned} \quad (17)$$

We here neglect the central-cell corrections [9–11], since these corrections including the electron-hole interaction become important at very small electron-hole distance $r \rightarrow 0$. Therefore, mostly even exciton states with a high percentage of an S state are affected. The number of S states compared to the total number of exciton states decreases strongly with increasing principal quantum number n . We therefore assume that central-cell corrections can be neglected in the semiclassical limit. This statement is supported by our classical computations, where we observe that the classical exciton orbits very rarely reach the region with small electron-hole distance $r \rightarrow 0$.

The band structure terms included in $H_{\text{kin}}(\mathbf{p}, \hat{\mathbf{I}}, \hat{\mathbf{S}}_h)$ depend quadratically on components p_i of the momentum, and therefore the scaling transformation (13) can still be applied to obtain an energy-independent classical dynamics. However, this does not hold for the spin-orbit coupling term

$$H_{\text{SO}} = \frac{2}{3}\Delta \left(1 + \frac{1}{\hbar^2} \hat{\mathbf{I}} \cdot \hat{\mathbf{S}}_h \right). \quad (18)$$

which does not depend on the momentum \mathbf{p} and thus depends on n_{eff} after multiplication of the total Hamiltonian by n_{eff}^2 . To recover the scaling property of the system we introduce a scaled version of the spin-orbit coupling by the replacement

$$\Delta \rightarrow \tilde{\Delta} = \frac{n_0^2}{n_{\text{eff}}^2} \Delta. \quad (19)$$

The dependence of the total Hamiltonian on n_{eff} can now be completely removed by the scaling, but the scaled classical dynamics depends on the constant factor n_0^2 , which determines the strength of the spin-orbit coupling. The classical dynamics of the scaled system corresponds exactly to that of the non-scaled crystal at energy $E = E_g - E_{\text{Ryd}}/n_{\text{eff}}^2$ with $n_{\text{eff}} = n_0$.

B. Adiabatic approach for the exciton dynamics

To calculate the classical dynamics of the yellow exciton series we resort to the adiabatic approach introduced in Ref. [12]. Thereby we assume that the fast motion of the spin degrees of freedom reacts instantaneously to a new configuration in the relative coordinates. The timescale of the spin dynamics is determined by the spin-orbit coupling Δ which is large already compared to the spacing of adjacent Rydberg states $2E_{\text{Ryd}}/n^3$ for principle quantum numbers $n \geq 3$. Diagonalizing the band structure part $H_{\text{band}}(\mathbf{p}, \hat{\mathbf{I}}, \hat{\mathbf{S}}_h)$ in a basis for quasispin and hole spin $|m_I, m_{S_h}\rangle$ with m_I and m_{S_h} the magnetic quantum numbers of the quasispin and hole spin, leads to three twofold degenerate energy surfaces in momentum space $W_i(\mathbf{p}, n_0)$. The lowest of those energy surfaces can be assigned to the yellow exciton series. To

interpret the fine-structure splitting of the yellow exciton series in cuprous oxide in terms of the classical exciton orbits, we have to choose the corresponding energy surface $W_1(\mathbf{p}, n_0)$. The Hamilton function is then given by

$$H = \frac{\gamma'_1}{2m_0} \mathbf{p}^2 + W_1(\mathbf{p}, n_0) - \frac{e^2}{4\pi\epsilon_0\epsilon|\mathbf{r}|}. \quad (20)$$

The classical exciton orbits are calculated by numerically integrating Hamilton's equations of motion

$$\dot{r}_i = \frac{\gamma'_1}{m_0} p_i + \frac{\partial W_1(\mathbf{p}, n_0)}{\partial p_i}, \quad \dot{p}_i = -\frac{e^2}{4\pi\epsilon_0\epsilon} \frac{r_i}{|\mathbf{r}|^3}. \quad (21)$$

Periodic orbits can be found by varying the initial conditions. We find periodic orbits confined to one- to three-dimensional tori. The one- and two-dimensional orbits are located in the two distinct symmetry planes of the crystal with O_h symmetry. The phase space exhibits mostly regular tori surrounding an elliptical fixed point given by a nearly circular orbit. The two-dimensional orbits show a secular motion of Kepler ellipses which can be characterized by two winding numbers M_1 and M_2 , whereby M_1 gives the number of Kepler ellipses and M_2 describes the secular motion by giving the number of circulations on the torus. For the three-dimensional orbits a third winding number needs to be included. M_2 then describes the secular motion in φ direction and M_3 describes the secular motion in ϑ direction.

Additional periodic orbit parameters, which are needed for the calculations of the semiclassical amplitudes, can be calculated by integrating the corresponding equations of motion simultaneously. The equation of motion for the action is given by

$$\frac{dS}{dt} = \mathbf{p} \frac{d\mathbf{r}}{dt}. \quad (22)$$

The stability properties of a periodic orbit are determined by the symplectic stability matrix \mathbf{M}_{po} , which is obtained by integrating

$$\frac{d}{dt} \mathbf{M} = \mathbf{J} \frac{\partial^2 H}{\partial \gamma \partial \gamma} \mathbf{M}, \quad \text{with } \mathbf{J} = \begin{pmatrix} \mathbf{0} & \mathbf{1} \\ -\mathbf{1} & \mathbf{0} \end{pmatrix}, \quad \gamma = \begin{pmatrix} \mathbf{r} \\ \mathbf{p} \end{pmatrix}, \quad (23)$$

over one period of the orbit with the initial condition $\mathbf{M}(0) = \mathbf{1}$. Due to the symplectic structure of the stability matrix its eigenvalues appear in pairs λ_i and $1/\lambda_i$.

For the nearly circular orbits all stability eigenvalues differ significantly from one. The direction out of the plane is stable for the orbit in the plane normal to $[100]$ and unstable for the orbit in the plane normal to $[1\bar{1}0]$. This behavior also holds for most of the two-dimensional orbits in the different symmetry planes. The direction out of the plane normal to $[1\bar{1}0]$ is unstable. By contrast, the stability out of the plane normal to $[100]$ shows stable behavior for most of the orbits in the symmetry plane. In the planes two partner orbits, one stable and one unstable orbit can be found in accordance with the Poincaré-Birkhoff theorem. However, the deviation of the stability

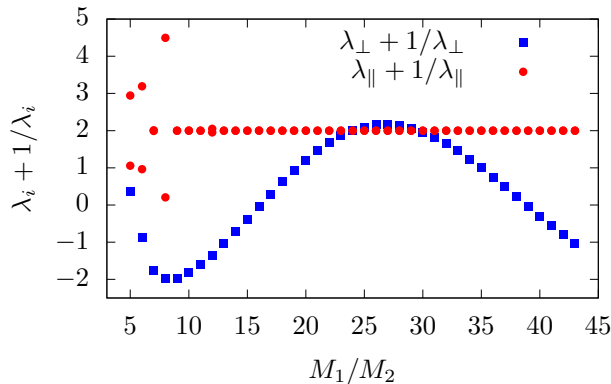


FIG. 1. Sum $\lambda_i + 1/\lambda_i$ for the two-dimensional orbits at $n_0 = 5$ in the plane normal to [100]. For the majority of orbits the deviation from stability eigenvalues $\lambda_i = 1$ cannot be resolved.

eigenvalues from one can only be resolved numerically for the orbits with the lowest ratios M_1/M_2 . This can be seen in Fig. 1 where the sums $\lambda_i + 1/\lambda_i$ are plotted over the ratio M_1/M_2 for the planar orbits normal to [100] for a fixed value $n_0 = 5$. $\lambda_{||}$ describes the stability of the orbit in the plane and λ_{\perp} the stability out of the plane. The majority of two-dimensional orbits exhibit one pair of stability eigenvalues with $\lambda_{||} = 1$. The same behavior can also be observed for the two-dimensional orbits in the other symmetry plane and for the three-dimensional orbits.

C. Calculation of the periodic orbit amplitudes

In this work we present results for $n_0 = 5$. This choice fixes the classical dynamics corresponding to the scaled exciton spectrum to that belonging to the exciton state at principal quantum number $n = 5$ in the non-scaled crystal. The value $n_0 = 5$ has been selected for two reasons. On the one hand, the secular motion of the classical exciton orbits in similar phase space regions becomes slower with increasing n_0 and non-trivial structures in the recurrence spectra occur only at higher values of the scaled action [13]. On the other hand, lower values $n_0 < 3$ belong to regions where the adiabatic approach introduced in Ref. [12] is no longer valid.

The one-dimensional orbits are isolated and their stability eigenvalues therefore differ from one. Their contribution to the density of states can be calculated by applying Gutzwiller's trace formula (5). However stability eigenvalues equal to one are typical for integrable systems where the density of states can be described by the Berry-Tabor formula. To calculate semiclassical amplitudes for two- and three-dimensional orbits we therefore replace the contributions of the directions belonging to stability eigenvalues $\lambda_i = 1$ in Gutzwiller's trace formula by the Berry-Tabor formula (4) for a two-dimensional integrable system. The contribution of the third direction

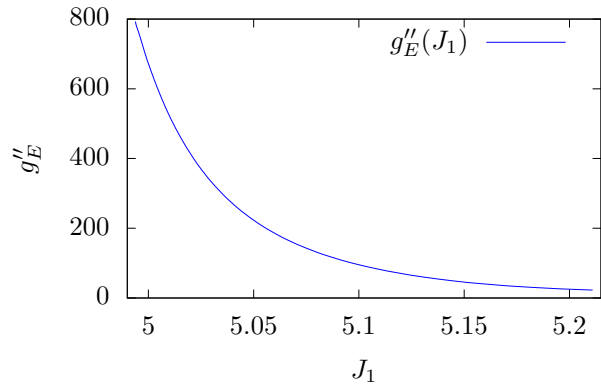


FIG. 2. Second derivative of the function $J_2 = g_E(J_1)$ with respect to J_1 at $n_0 = 5$. The orbits in the plane normal to [100] produce a steady curve which can be interpolated for orbits with intermediate values for J_1 and J_2 . All quantities are given in exciton-Hartree units which are obtained by setting $\hbar = e = m_0/\gamma'_1 = 1/(4\pi\epsilon_0\epsilon) = 1$.

is then given by a factor $1/\sqrt{|\lambda_{\text{po}} + 1/\lambda_{\text{po}} - 2|}$. The amplitudes for the two- and three-dimensional orbits then read

$$|\mathcal{A}_{\text{po}}| = \frac{1}{\pi\hbar} \frac{1}{\sqrt{|\lambda_{\text{po}} + 1/\lambda_{\text{po}} - 2|}} \frac{\tilde{S}_{\text{po}}}{\sqrt{\hbar M_2^3 |g''_E|}}. \quad (24)$$

To calculate these amplitudes the action variables J_1 and J_2 are needed. In a two-dimensional integrable system the action of a periodic orbit is given by

$$S_M = 2\pi(M_1 J_1 + M_2 J_2). \quad (25)$$

The action variables can then be calculated by differentiating Eq. (25) by the corresponding winding number M_i . For two-dimensional motion M_1 describes the number of Kepler ellipses, whereas M_2 describes the secular motion of an orbit. To describe the three-dimensional orbits within the same approach we treat them in an effective two-dimensional model by combining the contribution of the secular motion in ϑ direction described by M_2 and the secular motion in φ direction described by M_3 to give an overall contribution of the secular motion, which is then described by $\tilde{M}_2 = \text{GCD}(M_2, M_3)$. With the action variables J_1 and J_2 the function $J_2 = g_E(J_1)$ can be calculated. In Fig. 2 the second derivative g''_E with respect to J_1 is shown for the two-dimensional orbits in the plane normal to [100] for $n_0 = 5$. The amplitudes in Eq. (24) are calculated by choosing the g''_E of the corresponding orbit.

III. SCALED QUANTUM MECHANICAL EXCITON SPECTRA

In the quantum mechanical case the canonical commutation relations

$$[\hat{r}_i, \hat{p}_j] = i\hbar\delta_{ij} \quad (26)$$

must be satisfied. Inserting the scaled variables given in Eq. (13) yields

$$[\hat{r}_i, \hat{p}_j] = i \frac{\hbar}{n_{\text{eff}}} \delta_{ij}, \quad (27)$$

where the Planck constant is replaced by an effective Planck constant $\hbar_{\text{eff}} = \hbar/n_{\text{eff}}$. Using the corresponding operators in coordinate space given by

$$\hat{\mathbf{r}} = \tilde{\mathbf{r}}, \quad \hat{\mathbf{p}} = -i\hbar_{\text{eff}} \nabla_{\tilde{\mathbf{r}}}, \quad (28)$$

the Schrödinger equation for cuprous oxide can be transformed to the generalized eigenvalue problem

$$\begin{aligned} & \left[\frac{e^2}{4\pi\epsilon_0\epsilon|\mathbf{r}|} - n_0^2 H_{\text{SO}}(\hat{\mathbf{I}}, \hat{\mathbf{S}}_h) - E_{\text{Ryd}} \right] |\Psi\rangle \\ &= \frac{\hbar^2}{n_{\text{eff}}^2} H_{\text{kin}}(-i\nabla_{\tilde{\mathbf{r}}}, \hat{\mathbf{I}}, \hat{\mathbf{S}}_h) |\Psi\rangle \end{aligned} \quad (29)$$

for the effective quantum number n_{eff} .

A. Numerical solution of the generalized eigenvalue problem

To solve the generalized eigenvalue problem (29) we use the basis set

$$|\Pi\rangle = |N, L, J, F, M_F\rangle. \quad (30)$$

Here, N is the radial quantum number which is connected to the principal quantum number n via $N = n - L - 1$ and L the angular momentum quantum number. The quasispin I and the hole spin S_h are coupled via the spin-orbit coupling term H_{SO} to the effective hole spin J . The total angular momentum quantum number is denoted by $F = J + L$ and its z component by M_F . As we neglect the central-cell corrections affecting the even-parity states, the electron spin S_e and its z component M_{S_e} are good quantum numbers. They only result in additional degeneracies of the eigenstates and thus are not included in the basis (30).

For the radial part of the basis states we use the Coulomb-Sturmian functions [9]

$$U_{NL}(\tilde{r}) = N_{NL} (2\rho)^L e^{-\rho} L_N^{2L+1}(2\rho), \quad (31)$$

with the associated Laguerre polynomials $L_N^{2L+1}(x)$, $\rho = \tilde{r}/\alpha$, and α an arbitrary positive real-valued scaling parameter. The Coulomb-Sturmian functions form a discrete and complete set in $L^2(\mathbb{R}^3)$ independent of the scaling parameter $\alpha > 0$ [14–16]. The normalization factor N_{NL} reads

$$N_{NL} = \frac{2}{\sqrt{\alpha^3}} \left[\frac{N!}{(N+2L+1)!(N+L+1)!} \right]^{\frac{1}{2}}. \quad (32)$$

Note that the functions (31) are not orthogonal. For the angular parts of the basis states we use the spherical harmonics. For the eigenfunctions we use the ansatz

$$|\Psi\rangle = \sum_{N,L,J,F,M_F} c_{N,L,J,F,M_F} |\Pi\rangle, \quad (33)$$

with coefficients c . Using the ansatz (33) we can write the generalized eigenvalue problem in matrix form

$$\mathbf{A}\mathbf{c} = \lambda\mathbf{B}\mathbf{c}, \quad (34)$$

with symmetric matrices \mathbf{A} and \mathbf{B} , the solution vector \mathbf{c} , and the eigenvalues $\lambda = 1/n_{\text{eff}}^2$. The matrix elements of \mathbf{A} and \mathbf{B} ,

$$\begin{aligned} A_{\tilde{\Pi}\Pi} &= \langle \tilde{\Pi} | \left[\frac{e^2}{4\pi\epsilon_0\epsilon|\mathbf{r}|} - n_0^2 H_{\text{SO}}(\hat{\mathbf{I}}, \hat{\mathbf{S}}_h) - E_{\text{Ryd}} \right] | \Pi \rangle, \\ B_{\tilde{\Pi}\Pi} &= \langle \tilde{\Pi} | H_{\text{kin}}(-i\nabla_{\tilde{\mathbf{r}}}, \hat{\mathbf{I}}, \hat{\mathbf{S}}_h) | \Pi \rangle \end{aligned} \quad (35)$$

can be obtained analytically similar as in Ref. [17]. They have been adjusted to the basis set (30) using Clebsch–Gordan coefficients. The matrix equation (34) is set up using the basis set (30) with quantum numbers

$$\begin{aligned} L &= 0, \dots, n-1, \\ J &= 1/2, 3/2, \\ F &= |L-J|, \dots, L+J, \\ M_F &= -F, \dots, +F. \end{aligned} \quad (36)$$

As parity is a good quantum number, the generalized eigenvalue problem decomposes into two blocks with even and odd parity which corresponds to even and odd angular momentum L . Those blocks further decompose into four blocks because of the cubic symmetry of the kinetic part of the Hamiltonian H_{kin} and the quantization axis chosen parallel to one of the principal axis of the crystal. More precisely, as a rotation of 90° about a four-fold symmetry axis of the group O_h does not change the Hamiltonian and one of those axis coincides with the quantization axis it follows

$$\begin{aligned} \langle \Pi' | e^{\frac{iF_z\pi/2}{\hbar}} H_{\text{kin}} e^{-\frac{iF_z\pi/2}{\hbar}} | \Pi \rangle &= e^{\frac{i(M'_F - M_F)\pi/2}{\hbar}} \langle \Pi' | H_{\text{kin}} | \Pi \rangle \\ &= \langle \Pi' | H_{\text{kin}} | \Pi \rangle, \end{aligned} \quad (37)$$

which is only fulfilled if $M'_F - M_F = 4m$ with $m \in \mathbb{Z}$. Thus only states with $M_F = M'_F \pmod{4}$ couple. The four blocks correspond to the four equivalence classes of $M_F \pmod{4}$

$$\begin{aligned} [1/2] &= \{ \dots, -15/2, -7/2, 1/2, 9/2, 17/2, \dots \}, \\ [3/2] &= \{ \dots, -13/2, -5/2, 3/2, 11/2, 19/2, \dots \}, \\ [5/2] &= \{ \dots, -11/2, -3/2, 5/2, 13/2, 21/2, \dots \}, \\ [7/2] &= \{ \dots, -9/2, -1/2, 7/2, 15/2, 23/2, \dots \}. \end{aligned} \quad (38)$$

The symmetry of a state can be specified by the irreducible representations Γ_i of the cubic O_h group which determine the transformation behavior under symmetry

operations of the group. Because the angular momentum F is half-integer only the irreducible representations Γ_6, Γ_7 and Γ_8 appear [18]. The Γ_8 states are four-fold degenerate and one of those degenerate states appear in each block of Eq. (38). In the blocks [1/2] and [7/2] additionally only Γ_7 states, and in the blocks [3/2] and [5/2] additionally only Γ_6 states appear. Those Γ_6 and Γ_7 states are globally two-fold degenerate with one of the degenerate states in each block they occur in. Thus the block structure together with the degeneracy of the states can be used to assign the irreducible representation to a given state.

With the symmetry plane orthogonal to the four-fold axis along the z direction it follows that

$$\begin{aligned} & \langle N', L', J', F', M'_F | H_{\text{kin}} | N, L, J, F, M_F \rangle \\ &= \langle N', L', J', F', -M'_F | H_{\text{kin}} | N, L, J, F, -M_F \rangle, \end{aligned} \quad (39)$$

and thus for the matrices \mathbf{B} defined in Eq. (35)

$$\begin{aligned} \mathbf{B}_{M_F \in [1/2]} &\sim \mathbf{B}_{M_F \in [7/2]}, \\ \mathbf{B}_{M_F \in [3/2]} &\sim \mathbf{B}_{M_F \in [5/2]}, \end{aligned} \quad (40)$$

where \sim denotes similar matrices and thus their spectra are equal. They are similar because they can be transformed into each other by a basis transformation as only the arrangement of the basis vectors has to be changed. This explains the two-fold degeneracy of the Γ_6 and Γ_7 states. Thus the generalized eigenvalue problem (34) decomposes into four independent blocks, two for even and odd parity, respectively. This block structure is exploited to accelerate the numerical diagonalization using the LAPACK routine DSYGVX [19]. For the latter we need a finite basis and therefore set upper bounds n_{max} and L_{max} to the principal quantum number n and the angular momentum quantum number L , respectively. They are chosen sufficiently large to achieve convergence. The convergence parameter α is the same for all basis functions and can be used to enhance convergence. Our truncated basis set is therefore uniquely defined by the triple $(\alpha, n_{\text{max}}, L_{\text{max}})$.

B. Calculation of quantum mechanical recurrence spectra

The Fourier transform of the scaled quantum density of states

$$\varrho(n_{\text{eff}}) = \sum_k \delta(n_{\text{eff}} - n_{\text{eff},k}), \quad (41)$$

where $n_{\text{eff},k}$ denotes the k th eigenvalue of Eq. (34), should result in δ peaks at the scaled actions \tilde{S}_{po} and their repetitions. This is only valid for an infinite spectrum. For the finite one, resulting from the diagonalization of the truncated generalized eigenvalue problem, the δ peaks are broadened and side peaks occur. This can be seen as follows. The Fourier transform of the finite spectrum corresponds to that of the infinite one multiplied by a rectangular window function. With the convolution theorem this is equivalent to a convolution of the Fourier transformed infinite spectrum with

$$\frac{\sin(\Delta n_{\text{eff}} \tilde{S}_{\text{po}} / (2\hbar))}{\pi \tilde{S}_{\text{po}} / \hbar} e^{-in_{\text{eff}}^0 \tilde{S}_{\text{po}} / \hbar}, \quad (42)$$

where Δn_{eff} is the size of the window, i.e., the length of the finite spectrum, and n_{eff}^0 the center of the spectrum. To suppress the artificial side peaks a Gaussian window function

$$w(n_{\text{eff}}) \equiv \exp\left(-\frac{(n_{\text{eff}} - n_{\text{eff}}^0)^2}{2\sigma^2}\right) \quad (43)$$

is introduced with $\sigma = \Delta n_{\text{eff}}/6$. Unfortunately this further broadens the main peaks. For our calculations we used $n_{\text{eff}}^0 = 15$ and $\Delta n_{\text{eff}} = 30$. As the quantum spectrum is a sum of delta distributions the Fourier transform can be carried out analytically

$$\begin{aligned} \hat{C}(\tilde{S}) &= \frac{1}{2\pi} \sum_{k=1}^{k_{\text{max}}} \int_{\mathbb{R}} w(n_{\text{eff}}) \delta(n_{\text{eff}} - n_{\text{eff},k}) e^{-in_{\text{eff}} \tilde{S} / \hbar} dn_{\text{eff}} \\ &= \frac{1}{2\pi} \sum_{k=1}^{k_{\text{max}}} w(n_{\text{eff},k}) \left[\cos\left(n_{\text{eff},k} \tilde{S} / \hbar\right) - i \sin\left(n_{\text{eff},k} \tilde{S} / \hbar\right) \right], \end{aligned} \quad (44)$$

where $k = 1, \dots, k_{\text{max}}$ numerates the eigenvalues $n_{\text{eff},k}$ of the finite spectrum.

-
- [1] M. V. Berry and M. Tabor, Closed orbits and the regular bound spectrum, Proc. R. Soc. Lond. A **349**, 101 (1976).
 [2] S. Tomsovic, M. Grinberg, and D. Ullmo, Semiclassical trace formulas of near-integrable systems: Resonances, Phys. Rev. Lett. **75**, 4346 (1995).

- [3] M. C. Gutzwiller, *Chaos in Classical and Quantum Mechanics* (Springer, New York, 1990).
 [4] P. Cvitanović and B. Eckhardt, Periodic-orbit quantization of chaotic systems, Phys. Rev. Lett. **63**, 823 (1989).

- [5] A. Holle, J. Main, G. Wiebusch, H. Rottke, and K. H. Welge, Quasi-Landau spectrum of the chaotic diamagnetic hydrogen atom, *Phys. Rev. Lett.* **61**, 161 (1988).
- [6] H. Friedrich and H. Wintgen, The hydrogen atom in a uniform magnetic field – An example of chaos, *Physics Reports* **183**, 37–79 (1989).
- [7] J. Main, Use of harmonic inversion techniques in semiclassical quantization and analysis of quantum spectra, *Phys. Rep.* **316**, 233–338 (1999).
- [8] T. Kazimierczuk, D. Fröhlich, S. Scheel, H. Stolz, and M. Bayer, Giant Rydberg excitons in the copper oxide Cu_2O , *Nature* **514**, 343 (2014).
- [9] F. Schweiner, J. Main, G. Wunner, and C. Uihlein, Even exciton series in Cu_2O , *Phys. Rev. B* **95**, 195201 (2017).
- [10] A. Farenbruch, D. Fröhlich, D. R. Yakovlev, and M. Bayer, Rydberg series of dark excitons in Cu_2O , *Phys. Rev. Lett.* **125**, 207402 (2020).
- [11] P. Rommel, J. Main, A. Farenbruch, D. R. Yakovlev, and M. Bayer, Exchange interaction in the yellow exciton series of cuprous oxide, *Phys. Rev. B* **103**, 075202 (2021).
- [12] J. Ertl, P. Rommel, M. Mom, J. Main, and M. Bayer, Classical and semiclassical description of Rydberg excitons in cuprous oxide, *Phys. Rev. B* **101**, 241201(R) (2020).
- [13] M. Schumacher, *Semiclassical analysis and interpretation of quantum mechanically computed Cu_2O exciton spectra*, Master’s thesis, Universität Stuttgart (2021).
- [14] M. A. Caprio, P. Maris, and J. P. Vary, Coulomb-Sturmian basis for the nuclear many-body problem, *Phys. Rev. C* **86**, 034312 (2012).
- [15] B. Klahn and W. A. Bingel, The convergence of the Rayleigh-Ritz method in quantum chemistry I., *Theoretica Chimica Acta* **44**, 9 (1977).
- [16] B. Klahn and W. A. Bingel, The convergence of the Rayleigh-Ritz method in quantum chemistry II., *Theoretica Chimica Acta* **44**, 27 (1977).
- [17] F. Schweiner, J. Main, M. Feldmaier, G. Wunner, and C. Uihlein, Impact of the valence band structure of Cu_2O on excitonic spectra, *Phys. Rev. B* **93**, 195203 (2016).
- [18] G. Koster, J. Dimmock, R. Wheeler, and H. Statz, *Properties of the thirty-two point groups*, Massachusetts Institute of Technology Press research monograph (M.I.T. Press, Cambridge, 1963).
- [19] E. Anderson, Z. Bai, C. Bischof, S. Blackford, J. Demmel, J. Dongarra, J. D. Croz, A. Greenbaum, S. Hammarling, and A. McKenney, *LAPACK Users’ Guide, Third edition* (Society for Industrial and Applied Mathematics, Philadelphia, 1999).